

International Conference on Computational Science, ICCS 2011

# Visualizing Life Zone Boundary Sensitivities Across Climate Models and Temporal Spans

Robert Sisneros<sup>a</sup>, Jian Huang<sup>b</sup>, George Ostrouchov<sup>a</sup>, Forrest Hoffman<sup>a</sup>

<sup>a</sup>Oak Ridge National Laboratory, Oak Ridge, TN 37831, USA

<sup>b</sup>University of Tennessee, Knoxville, TN 37996, USA

---

## Abstract

Life zones are a convenient and quantifiable method for delineating areas with similar plant and animal communities based on bioclimatic conditions. Such ecoregionalization techniques have proved useful for defining habitats and for studying how these habitats may shift due to environmental change. The ecological impacts of climate change are of particular interest. Here we show that visualizations of the geographic projection of life zones may be applied to the investigation of potential ecological impacts of climate change using the results of global climate model simulations. Using a multi-factor classification scheme, we show how life zones change over time based on quantitative model results into the next century. Using two straightforward metrics, we identify regions of high sensitivity to climate changes from two global climate simulations under two different greenhouse gas emissions scenarios. Finally, we identify how preferred human habitats may shift under these scenarios. We apply visualization methods developed for the purpose of displaying multivariate relationships within data, especially for situations that involve a large number of concurrent relationships. Our method is based on the concept of multivariate classification, and is implemented directly in VisIt, a production quality visualization package.

*Keywords:* visualization, life zones, climate change, climate modeling, multivariate classification

---

## 1. Introduction

When studying complex natural phenomena, it is very important to distinguish the normal vs. the unexpected. It is important to have the right set of tools to properly identify deviations from an expected pattern in the context of many possible alternative situations. This question is very hard to answer in general. Beginning with methods developed in [1], we expand these capabilities to study complex relationships resulting from global climate change modeling.

In particular, we apply our methods to the study of the sensitivities of life zone boundary changes across multiple climate change projections under different emissions scenarios. Our visualization technique provides a user-guided way of concurrently and interactively controlling classification of more than 30 possible multivariate states. The user control that is allowed is more powerful and more effective than previous systems, yet without compromising

---

*Email addresses:* [rjsisneros@ornl.gov](mailto:rjsisneros@ornl.gov) (Robert Sisneros), [huangj@eecs.utk.edu](mailto:huangj@eecs.utk.edu) (Jian Huang), [ostrouchovg@ornl.gov](mailto:ostrouchovg@ornl.gov) (George Ostrouchov), [forrest@climatemodeling.org](mailto:forrest@climatemodeling.org) (Forrest Hoffman)

convenience or scalability. Our classification system is also designed to handle application domains that require non-trivial statistical methods, such as the definition and visualization of life zones.

The concept of life zones was first developed by C. Hart Merriam in 1889 as a convenient way of delineating areas with similar plant and animal communities. In 1947, Leslie Holdridge defined life zones in a quantitative way based on empirical global bioclimate data [2, 3]. When mapped onto the Earth, the Holdridge life zones constitute generalized plant and animal habitats, assuming that soil properties and climate vegetation are broadly determined by predominate climate conditions. Ecologists commonly use such ecoregionalization schemes to define and study biomes, and to investigate potential impacts of climate change on plant and animal species ranges. Life zones have also been used for studying issues that arise in climate models, such as time scales [4] and spatial resolutions [5].

Here we apply the Holdridge life zone classification scheme to visualize the results from two 100-year climate change simulations based on two strategically chosen scenarios of greenhouse gas emissions. We demonstrate the utility of ecoregionalization for studying the influence of climate change on habitats and definitively visualize the ways and the degree in which life zones may grow, shrink, or shift across the landscape in the coming century depending on emission scenarios. Furthermore, we show these results together with two statistical metrics that reveal regions highly sensitive to climate change. In this process, we also validate the effectiveness of interactively controlled classification for studying relationships within complex multivariate problem spaces.

## 2. Background

In this section, we begin with a description of the system for the classification of land area that we use as an input to our visualization scheme. We then introduce our target analysis data, along with differentiating emissions scenarios. Finally, we detail the visualization approach for the classification of data via high dimensional target areas.

### 2.1. Holdridge Life Zones

Holdridge life zones [2, 3] refer to a system for classifying land areas of the globe based on surface atmospheric conditions. Although originally developed for use in tropical/subtropical areas, the system is globally applicable and has even been used to analyze vegetation pattern alterations due to global warming [6]. Our specification of target areas and resulting classification based on those targets naturally implement this classification system.

The target areas are specified in terms of three climatic measurements: biotemperature, annual precipitation, and the ratio of potential evapotranspiration (PET) to annual precipitation; all of these may be seen in Figure 1. Biotemperature is a measure of energy that a plant can use. It differs from actual temperature in that all temperatures below/above a certain minimum/maximum are considered identical to that minimum/maximum. This reflects the concept that plants receive no energy below the minimum and cannot utilize more energy from temperatures above the maximum [3]. PET is the measure of the total possible evaporation and transpiration if water were unlimited, and the ratio of PET to annual precipitation is an aridity index: the greater precipitation is than PET the more humid an area, while greater PET values correspond to more arid areas.

The space in which the Holdridge life zones are defined is not orthogonal. For instance, the PET ratio depends on both annual precipitation and biotemperature. In fact, a life zone in Figure 1 may be indexed by any two of the three climatic measurements. However, when considering actual data, different choices of the two measurements may lead to different mappings. This is also noted in [7] and solved with a “fuzzy” adjustment on one coordinate. We address this by the Voronoi tessellation [8] generated by our three dimensional targets. All three climatic measurements define the life zones on a logarithmic scale. Holdridge based this on well known Mitscherlich yield studies, which found equal increases in yield in response to doubling of a limiting nutrient (see for example, [9]). As the life zones are defined by upper and lower bounds on each of the three variables, our targets are simply the geometric averages of these bounds, which are the centroids of the life zone hexagons after the log transformation.

### 2.2. Community Climate System Model (CCSM)

Climate model simulation results used in this analysis were generated by the National Center for Atmospheric Research (NCAR) Community Climate System Model version 3 (CCSM3) [11] for the Third Climate Model Inter-comparison Project (CMIP3). These simulations were analyzed as a part of the Intergovernmental Panel on Climate Change (IPCC) Fourth Assessment Report (AR4). CCSM3 is a climate modeling system that includes component

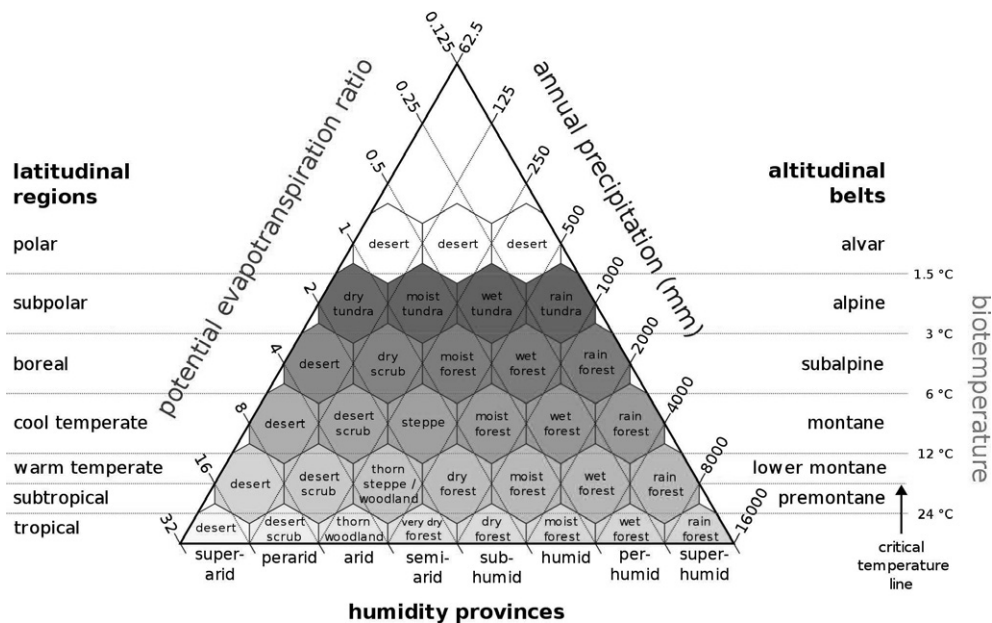


Figure 1: Canonical representation of the Holdridge life zones [10].

models representing the atmosphere, oceans, land surface, and sea ice, coupled together into a single integrated system that runs primarily on supercomputers and parallel distributed memory compute clusters. CCSM3 is designed as a basic research tool useful for understanding Earth's past, present, and future climate states. For the CMIP3 simulations used here, CCSM3 was run using a Gaussian grid with 128 latitude and 256 longitude points for the atmosphere and land components and a variable one-degree grid for the ocean and sea ice components. The CCSM3 simulation results used in this study were obtained from the Earth System Grid (ESG) at the U.S. Dept. of Energy's Program for Climate Model Diagnosis and Intercomparison (PCMDI). These data were downloaded from <http://www.earthsystemgrid.org/>.

### 2.3. Emissions Scenarios

To determine the sensitivities of life zone boundaries under possible climate change conditions at the end of the next century, results from simulations following two different greenhouse gas emissions scenarios were chosen for analysis. These two scenarios, labeled A2 and B1, represent high and low global emissions of radiatively active greenhouse gases over the twenty-first century, respectively. As a result, the shift in life zone regions from these two model projections should bound expected changes in ecological habitats with minor shifts under the B1 scenario and more significant shifts under the A2 scenario. The storylines for both scenarios are described in detail in [12], but are summarized as follows.

The A2 storyline and scenario family describes a heterogeneous world with a continuously increasing population. The underlying theme is self-reliance and preservation of local identities. Economic development is primarily regionally oriented and per capita economic growth and technological change are more fragmented and slower than in other storylines. The B1 storyline and scenario family describes a convergent world with a global population that peaks around 2050 and declines thereafter. Economic structures change toward a service and information economy, with reductions in material intensity and the introduction of clean and resource-efficient technologies. The emphasis is on global solutions to economic, social, and environmental sustainability, including improved equity, but without climate initiatives that implement emissions targets like those specified by the Kyoto Protocol.

### 2.4. Visualizing Multidimensional Relationships

In [1] the authors present an approach for classifying high-dimensional data, and presenting the results in a single summary. Classifiers are user-defined and take the form of values of interest for a specific variable, or *target values*.

	Ann. Precip. (mm)	Biotemp. (C)	PET Ratio		Ann. Precip. (mm)	Biotemp. (C)	PET Ratio
1 Polar Desert	88.388	0.000	0.707	18 Rain Forest	2828.427	8.485	0.177
2 Polar Desert	176.777	0.000	0.354	19 Subtropical Desert	88.388	16.971	11.314
3 Polar Desert	353.553	0.000	0.177	20 Desert Scrub	176.777	16.971	5.657
4 Dry Tundra	88.388	2.121	1.414	21 Thorn Steppe/Woodland	353.553	16.971	2.828
5 Moist Tundra	176.777	2.121	0.707	22 Dry Forest	707.107	16.971	1.414
6 Wet Tundra	353.553	2.121	0.354	23 Moist Forest	1414.214	16.971	0.707
7 Rain Tundra	707.107	2.121	0.177	24 Wet Forest	2828.427	16.971	0.354
8 Boreal Desert	88.388	4.243	2.828	25 Rain Forest	5656.854	16.971	0.177
9 Dry Scrub	176.777	4.243	1.414	26 Tropical Desert	88.388	26.833	22.627
10 Moist Forest	353.553	4.243	0.707	27 Desert Scrub	176.777	26.833	11.314
11 Wet Forest	707.107	4.243	0.354	28 Thorn Woodland	353.553	26.833	5.657
12 Rain Forest	1414.214	4.243	0.177	29 Very Dry Forest	707.107	26.833	2.828
13 Montane Desert	88.388	8.485	5.657	30 Dry Forest	1414.214	26.833	1.414
14 Desert Scrub	176.777	8.485	2.828	31 Moist Forest	2828.427	26.833	0.707
15 Steppe	353.553	8.485	1.414	32 Wet Forest	5656.854	26.833	0.354
16 Moist Forest	707.107	8.485	0.707	33 Rain Forest	11313.709	26.833	0.177
17 Wet Forest	1414.214	8.485	0.354				

Figure 2: Color key for our life zone visualizations including actual values for the geometric centroids. Life zones are numbered as in the histograms of Figure 4.

The summary visualization is then over this set of classifiers, with one chosen at each spatial location. The target value chosen is the one with minimum Euclidean distance calculated in a probability density space to favor outliers.

In this work we are using an augmented version of the method outlined in [1]. Results are now produced by classifying each spatial location of the input dataset as belonging to one of several user-specified high-dimensional targets. These targets sets of points which together form the logical notion of an inter-variable relationship. In addition, the space in which distances are calculated are abstracted, as well as the distance metric used. Our classification system therefore easily accommodates what was intended by Holdridge life zones by an initial log transformation of targets and coordinate attributes so that distances are calculated on a log scale; the distance metric is still Euclidean.

This method acts on data as an *operator* within VisIt, and has been implemented to leverage VisIt's parallel and distributed architecture to maintain interactivity of rendering. Upon application of the operator on the data, the user is presented an interface for both the specification of target areas as well as the selection of calculation spaces and distance metrics. Our classification process is summarized as the following: VisIt reads the data, the user applies the operator (our method) to the data and selects the type of plot into which VisIt will place the results. The user interacts with the data through this operator, and can specify any number of relationships, define distance calculations and then simply request VisIt to display the results. In general, high dimensional relationships are complex and difficult to interpret, so our approach first aims for a trial-and-error process where the user has fully interactive control of relationship specifications and can discover salient features on the fly through fully interactive visualization. Second, our approach provides a way to summarize a large number of relationships in each visualization. In this work, we start with a (large) set of pre-defined relationships that are well known and useful. Through summary visualization, we allow user to evaluate and control these relationships simultaneously. The visualizations are easily customizable and animated through time using VisIt's gui and plot interfaces. This overall setting aids in analyzing the trends of relationships over time and in finding areas where extreme or dominant events are occurring. Also, the ability to reduce a large amount of data in to single images leads to efficient navigation toward concise areas of interest, which is particularly useful when analyzing climate data.

Separate from our work, many other researchers have studied multivariate visualization as well. To our knowledge, few other methods can offer concurrent and interactive control of 30 relationships in high dimensional spaces. Kniss et al. [13] developed a method where users specify centroids of multivariate targets as well as the radius around each target. Although we still resort to thresholding for filtering out samples far from all multivariate relationship targets, our method removes the requirement of those relationship-specific radius settings that are very hard to pick for explorative tasks. Our method in essence computes a Voronoi partition [8] of the space to more comprehensively classify the problem space. Also unlike previous works, we use distance metrics in probability space to automatically and transparently help users to address the effects of “what is normal” vs. “what is abnormal”.

Many information visualization works have also looked at classifying multivariate relationships using methods such as scatter plots and parallel coordinates [14, 15, 16]. While we consider those works inspirational, our targeted study is scientific datasets, where relationships or patterns exist in a location and time specific manner, as opposed to being globally uniform. It is very important for us to “see” relationships on their native grid in a snap shot and simultaneously comprehend, confirm and evaluate the existence of many multivariate relationships.

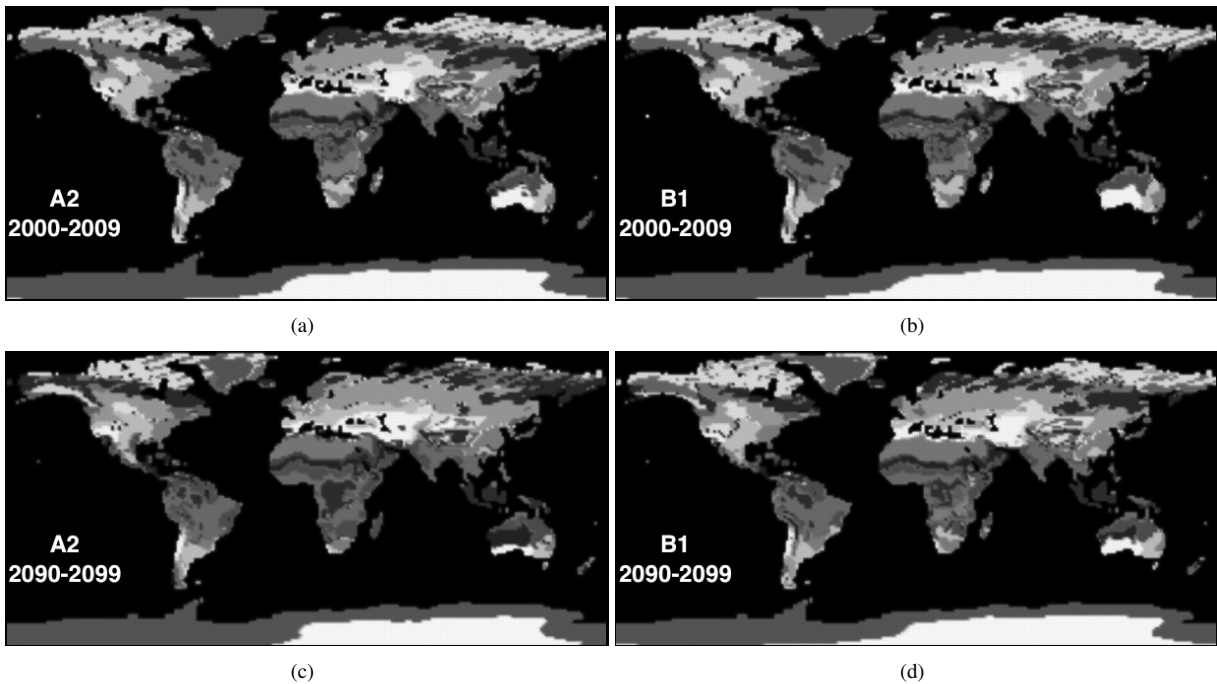


Figure 3: Life zone classifications of the present (2000–2009) for A2 (a) and B1 (b), and the future (2090–2099) for A2 (c) and B1 (d).

### 3. Approach

#### 3.1. Life Zones in CCSM

The three variables defining life zones are not calculated in the CCSM simulations, but are readily derived from other variables in CCSM. Biotemperature was calculated from CCSM's 2-meter air temperature (TSA), which is converted to degrees celsius, constrained to the range  $[0, 30]$  and averaged yearly. Annual precipitation was calculated as the sum of all rain (RAIN) and snow (SNOW) and converted from  $\text{mm s}^{-1}$  to mm. Lastly, we calculate our PET by Thornthwaite's original PET estimation [17]:

$$\text{PET} = 1.6 \left( \frac{L}{12} \right) \left( \frac{N}{30} \right) \left( \frac{10T_a}{I} \right)^\alpha$$

$$\alpha = (6.75 \times 10^{-7})I^3 - (7.71 \times 10^{-5})I^2 + (1.792 \times 10^{-2})I + 0.49239$$

$$I = \sum_{i=1}^{12} \left( \frac{T_{ai}}{5} \right)^{1.514}$$

where  $T_a$  is the monthly average of temperature and  $T_{ai}$  is the 12 monthly mean temperatures for the year.  $N$  is the number of days for the current month being calculated, and  $L$  is the average length of the day for the month. All of this is readily calculated directly from the CCSM data from TSA except  $L$ :

$$L = 24 \left( \frac{\arccos(1-m)}{180} \right)$$

$$m = 1 - \tan(Lat) \tan \left( Axis \times \cos \left( \frac{\pi \times Day}{182.625} \right) \right)$$

Where  $Axis$  is a constant (23.439), an estimation of the obliquity of the ecliptic. The CCSM variable needed to calculate  $L$  is the latitude at each spatial location ([http://herbert.gandraxa.com/length\\_of\\_day.aspx](http://herbert.gandraxa.com/length_of_day.aspx)).

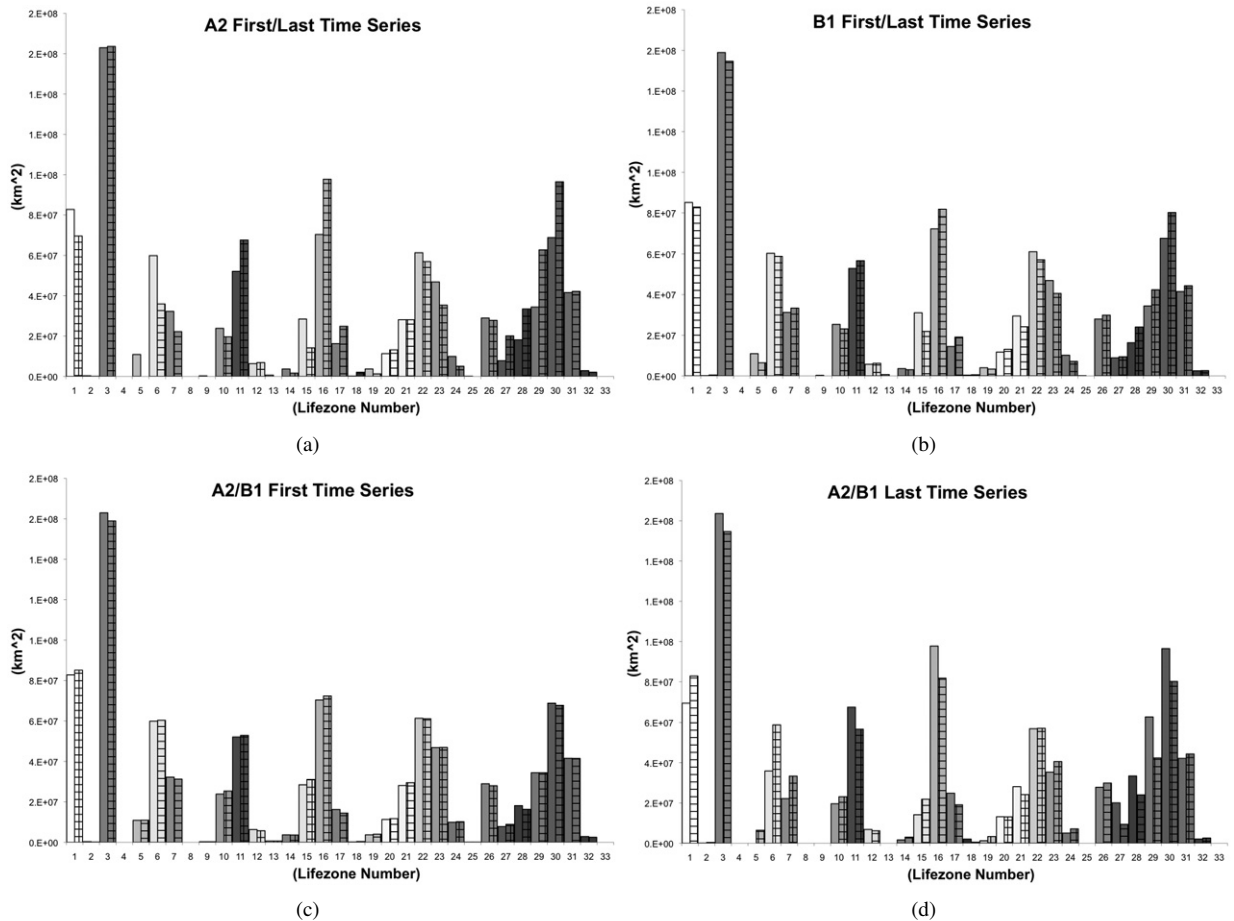


Figure 4: Histograms showing the distribution of land areas classified into each life zone. The  $x$  and  $y$  axes are life zone numbers and land area, respectively. The clear/shaded bars in (a) show the classification distribution for the present (2000–2009)/future (2090–2099) decades for the A2 scenario simulation. The same is shown for the B1 scenario simulation in (b). The clear/shaded bars in (c) show the classification distribution for the present (2000–2009) decade for the A2/B1 scenario simulations. The same is shown for the future (2090–2099) decade for the A2/B1 scenario simulations in (d).

It is clear that some properties of the variables are ignored, e.g. co-occurrence of statistical extremes and frequency and timing of those co-occurrences. Holdridge's life zones give only a general overview of environmental suitability; this represents an important challenge for future work.

Finally, we compute decadal averages for the three derived variables, and specifically focus on the averages of 2000–2009 and 2090–2099.

### 3.2. Visualizing Life Zones

There is some similarity of our proposed visualization approach to the technique used in  $k$ -means clustering [18]. It is equivalent to the “assignment step,” where items are assigned to their nearest means. The primary difference from a  $k$ -means algorithm is that our targets are user-specified, in this case they are simply the Holdridge life zone specifications, rather than estimated from the data [19, 20, 21]. These two types of approaches were compared in [22]. A further difference is that our distance computation takes place on a logarithmic scale where the geometric centroids become arithmetic centroids. The resulting Voronoi tessellation of the three-measurement space into life zones is a self-consistent representation that approximates the graphical rendering of Holdridge life zones in Figure 1. Due to the nature of the specification of the life zones, they are an ideal subject for our visualization approach. Figure 2

details the numbering from 0 to 33 and name of each life zone. It also specifies the color of each life zone as it is represented in our classification results as well as the geometric centroids for each life zone.

#### 4. Results

Using our visualization approach, the functionality needed to concurrently view 33 separate three-dimensional relationships is readily available. Figure 3 shows the result of classifying both the A2 and B1 scenario simulation results for the 33 life zones shown in Figure 2. For each scenario, the classification is done for the average of the first (2000–2009) and last (2090–2099) decades of the model simulations. Although all life zones are specified in input, not all are present in Figure 3, the output. Life zones are pre-defined by observed data, and therefore are likely not general to our simulation data. Figure 4 shows the actual distribution of the life zones after classification, and more clearly illuminates which life zones are not found in our data.

The geographic projection of these visualized life zones appears consistent with maps of ecoregions commonly employed by ecologists. Shifts in life zone regions between the present (Figure 3(a) and (b)) and future (Figure 3(c) and (d)) decadal averages due to climate change is evident in model results from both scenarios. Because both model simulations began from the end of the same historical simulation, there are few differences between the life zone maps of the present decade (Figures 3(a) and (b)). However, significant differences appear in the maps of future life zones under the two different emissions scenarios (Figures 3(c) and (d)).

Under the A2 scenario, the model projects sizable decreases in global coverage of polar deserts and wet tundra, and increases in wet forest, moist forest, thorn woodland (particularly in Central Western Australia), and dry forest. These results are consistent with global increases in temperature, especially at high latitudes, and shifting hydrological regimes. The coastlines of Greenland shift from polar desert to tundra. In addition, life zones in Northern Hemisphere mid- to high-latitudes exhibit an overall shift poleward. The changes in areal coverage can be seen in the histogram of land areas for the A2 scenario shown in Figure 4(a). Under the B1 scenario, the model projects similar but smaller shifts in life zones, consistent with less significant increases in temperature. For instance, the conversion of Greenland coastlines to tundra are less significant in B1 than in A2, and Siberia does not experience the nearly complete loss of tundra in B1 as it does in A2. The changes in areal coverage for the B1 scenario are shown in the histogram of land areas in Figure 4(b). The histogram in Figure 4(c) shows the minor differences between the present (2000–2009) A2 and B1 simulations, while the histogram in Figure 4(d) shows the more significant differences between the A2 and B1 simulations for the future (2090–2099).

##### 4.1. Sensitivity Analysis

In this section, we investigate the sensitivity of the classification across all decades from 2000–2099 via the calculation of two sensitivity metrics and the comparison of these metrics applied to the simulation results for both emissions scenarios. First, to identify regions that may be especially sensitive to changes in climate, we calculate the “persistence” of the life zone classifications for every decade between 2000–2099 for each spatial location. Regions that are classified into many different life zones in those nine decades are considered to be especially sensitive to climate change, while regions that are classified into a single life zone in each of those nine decades are considered to be relatively insensitive to changes in climate. Results for this “persistence” metric are shown in Figure 5 for the A2 and B1 scenario simulations. In this figure, white areas have the highest persistence (*i.e.*, a single unique life zone classification), blue areas have high persistence and relatively low sensitivity (*i.e.*, few unique life zone classifications) and red areas have low persistence and high sensitivity (*i.e.*, many unique life zone classifications). As expected, the A2 scenario simulation exhibits lower overall persistence than the B1 scenario simulation. It is also evident that there are latitudinal features in Figure 5. These reinforce the intuitive notion that the areas between life zones are those exhibiting the greatest number of changes. A possible contributing factor to this occurrence may be that points that lie on the boundary between two life zones easily swap between the two. We hence need to analyze this metric along side one that provides insight as to the significance of the changes as well.

Our second metric is a relative measure of the overall magnitude of change between the first (2000–2009) and last (2090–2099) decades, we calculate the Euclidean distance between the centroid of the first life zone and the last life zone into which each spatial location is classified. This “magnitude of change” metric, which is calculated in the log of the 3-dimensional phase space, highlights the regions most sensitive to changes in climate according to

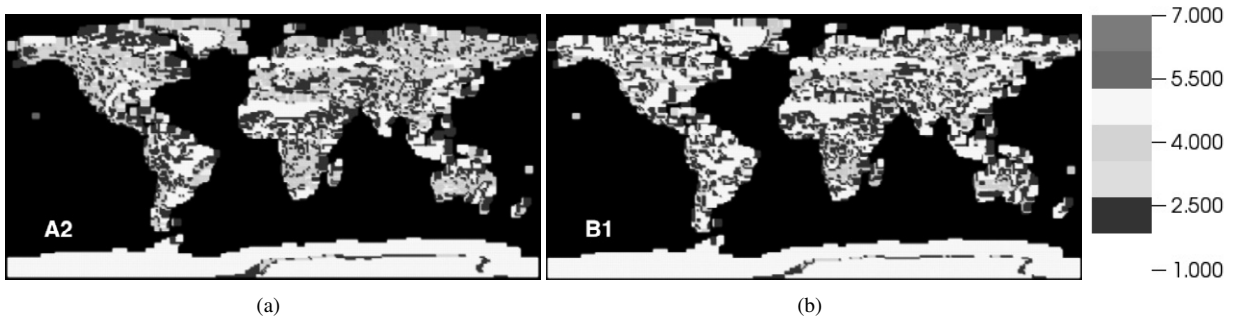


Figure 5: The “persistence” metric: A count of the total number of unique life zones seen at each location over all decades (2000–2099) for the A2 (a), and the B1 (c) scenario simulations.

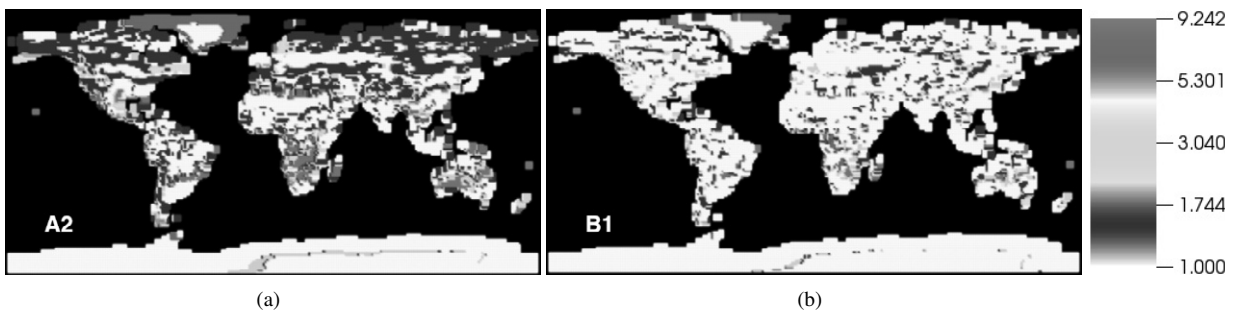


Figure 6: The “magnitude of change” metric: The Euclidean distance between the life zone centroids for the present (2000–2009) and the future (2090–2099) decades under the A2 (a) and B1 (b) scenarios.

how significant those changes are. Maps of the results for both scenarios are shown in Figure 6. In this figure, white regions do not change, blue regions change by a relatively small distance in the 3-dimensional phase space, and red regions shift by a large distance in the 3-dimensional phase space. As expected, the overall magnitude of change is much greater for the A2 scenario simulation than for the B1 scenario simulation, with the largest changes occurring primarily in high latitude regions.

To further compare the results of these metrics between the two scenario simulations, the differences between the A2 and B1 metrics are directly visualized. Figure 7 (a) shows the difference between the two “persistence” metric images in Figure 5. Regions that experience the same number of unique life zones (although likely different transitions) in each decade across both simulations are shown in white. It is the colored regions, however, that give insight into the comparison of scenarios. Regions shown in red exhibited lower persistence and higher sensitivity under the A2 scenario, while regions shown in blue exhibited lower persistence and higher sensitivity under the B1 scenario. This comparison suggests that some regions, like northeastern Greenland and some mid-latitude areas, realize more life zone transitions under the more slowly changing climate conditions of the B1 emissions scenario. Similarly, Figure 7 (b) shows the difference between the two “magnitude of change” metric images in Figure 6. Regions shown in white represent identical distance in phase space across both scenarios. Red regions experienced a larger change or more sensitivity under the A2 scenario, while regions shown in blue experienced a larger change or more sensitivity under the B1 scenario. This comparison suggests that a few mid-latitude regions may exhibit larger shifts in life zones under the less severe climate change realized under the B1 emissions scenario. Both of these scenario comparisons tend to highlight the boundaries between life zones, which are the land areas likely to change the most under changing climate conditions, confirming that life zone boundaries are the regions most sensitive to climate change.

#### 4.2. Comfortable Places to Live

Holdridge, in his work [3], states that life zones bordering the PET ratio of 1 are the most comfortable places in which to live. Figure 8 contains a visualization with an extra operator, a threshold on PET with a range of 0.5 to 2.0,

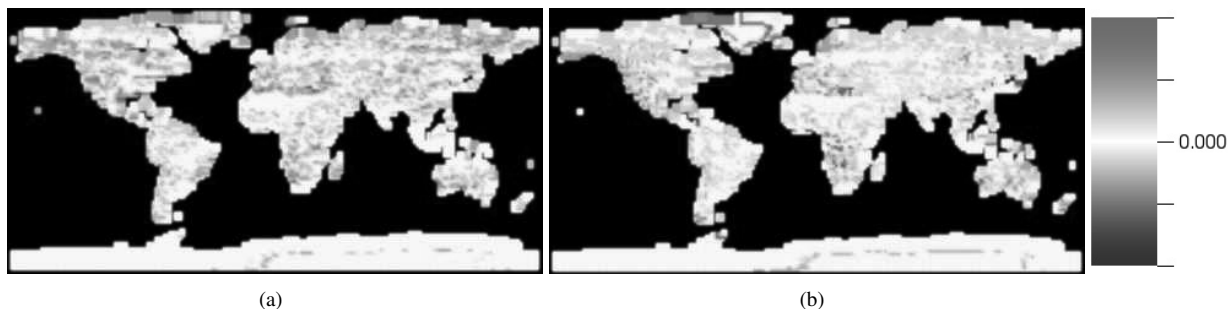


Figure 7: The most sensitive scenario: (a) the difference between the “persistence” metric for the A2 and B1 scenario simulations, and (b) the difference between the “magnitude of change” metric for the A2 and B1 scenario simulations. White regions experience the same number of life zone changes or magnitude of change. Red regions experienced more unique life zones or larger changes under the A2 scenario. Blue regions experienced more unique life zones or larger changes under the B1 scenario.

added to VisIt’s pipeline. This overview and drill-down process shows the relevant areas from Figure 3 for both the A2 and B1 scenario simulations, and for both the present (2000–2009) and future (2090–2099) decades of the simulations. White areas in these maps have a PET ratio outside this “comfortable” range. Non-white areas are colored by their life zone classification. Under both the A2 and B1 scenarios, about 40% of the land area has a PET ratio near 1 in the present (2000–2009) decade. In the future (2090–2099) decade under both scenarios, the regions have shifted and the land surface area in the comfortable range has been reduced. Under the B1 scenario, the comfortable land area is reduced by less than half a percent from present, while under the A2 scenario, the comfortable land area is reduced by nearly 3% from present. Under the A2 scenario, large regions in the southern part of North America and tropical South America depart from the comfortable range in the future. These results suggest that conservation efforts should consider climate conditions when establishing habitats for preservation.

## 5. Conclusion

We have demonstrated a powerful method for exploring climate model predictions and interpreting the impact of projected climate change on habitats through visualization. Using a multi-factor classification scheme, we have projected Holdridge life zone classifications onto land areas for the present and future under two different greenhouse gas emissions scenarios. We have shown that two straightforward metrics can identify regions of high sensitivity to climate change. The “persistence” metric highlights regions that experience many life zone changes through time. The “magnitude of change” metric highlights regions that exhibit large shift in the factors considered in life zone classifications. The results of applying these metrics suggest that borders between life zones are the most sensitive to climate change.

## References

- [1] R. Sisneros, C. R. Johnson, J. Huang, Concurrent viewing of multiple attribute-specific subspaces, *Computer Graphics Forum* (special issue for EuroVis) 27 (3) (2008) 783–790.
- [2] L. R. Holdridge, Determination of world plant formations from simple climatic data, *Science* 105 (2727) (1947) 367–368.
- [3] L. Holdridge, *Life Zone Ecology*, Tropical Science Center, San Jose, Costa Rica, 1967.
- [4] C. Ciret, A. Henderson-Sellers, ‘static’ vegetation and dynamic global climate: Preliminary analysis of the issues time steps and time scales, *Journal of Biogeography* 22 (4/5) pp. 843–856.
- [5] C. Ciret, A. Henderson-Sellers, Sensitivity of ecosystem models to the spatial resolution of the near community climate model ccm2, *Climate Dynamics* 14 409–429.
- [6] R. Leemans, Possible Changes in Natural Vegetation Patterns Due to a Global Warming, International Institute of Applied Systems Analysis, Laxenburg, Austria, 1990, IIASA Working Paper WP90-08 and Publication Number 108 of the Biosphere Dynamics Project.
- [7] A. E. Lugo, S. L. Brown, R. Dodson, T. S. Smith, H. H. Shugart, The Holdridge life zones of the conterminous United States in relation to ecosystem mapping, *J. Biogeogr.* 26 (1999) 1025–1038.
- [8] Q. Du, V. Faber, M. Gunzburger, Centroidal voronoi tessellations: Applications and algorithms, *SIAM Review* 41 (1999) 637–676.
- [9] C. A. Black, *Soil fertility evaluation and control*, CRC Press, 1992.

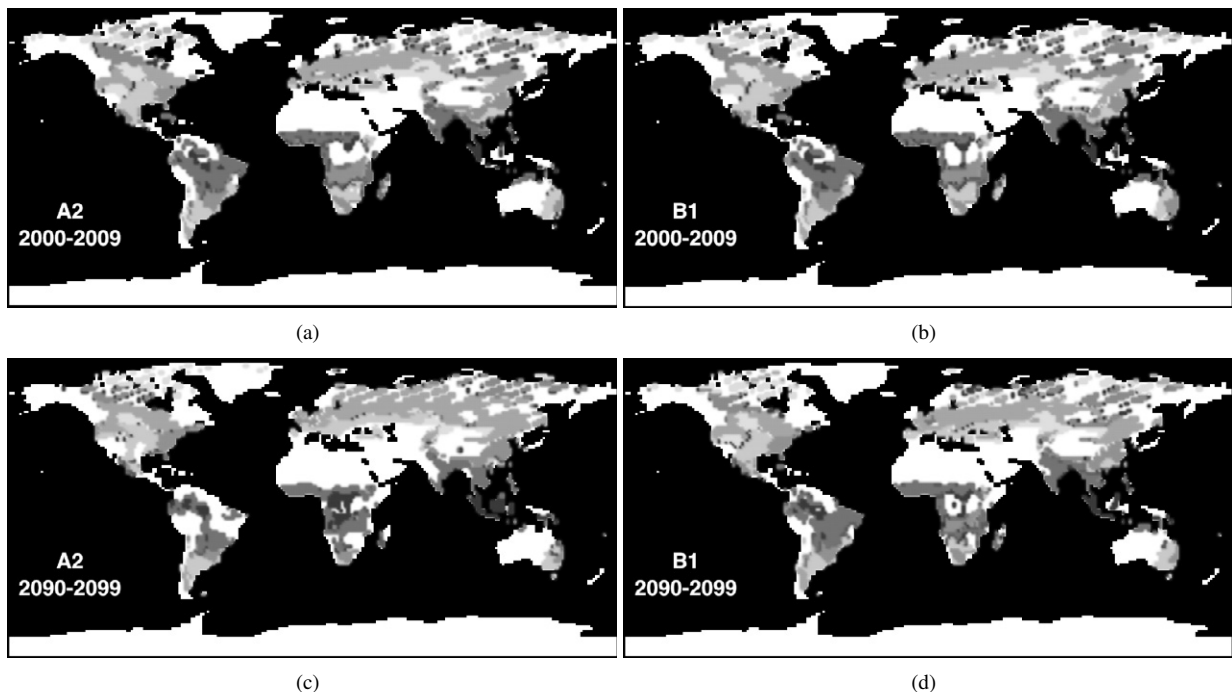


Figure 8: Life zones bordering PET ratio of 1 for the present (2000–2009) decade under the A2 scenario (a) and under the B1 scenario (b). Life zones bordering PET ratio of 1 for future (2090–2099) decade under the A2 scenario (c) and under the B1 scenario (d).

- [10] P. Halasz, Holdridge life zone, <http://en.wikipedia.org/wiki/File:Lifezones.Pengo.svg>, downloaded Jan 29, 2011, Permission: Creative Commons BY SA (any version) (3 March 2007).
- [11] W. D. Collins, C. M. Bitz, M. L. Blackmon, G. B. Bonan, C. S. Bretherton, J. A. Carton, P. Chang, S. C. Doney, J. J. Hack, T. B. Henderson, J. T. Kiehl, W. G. Large, D. S. McKenna, B. D. Santer, R. D. Smith, The Community Climate System Model version 3 (CCSM3), *J. Clim.* 19 (11) (2006) 2122–2143.
- [12] N. Nakićenović, J. Alcamo, G. Davis, B. de Vries, J. Fenhann, S. Gaffin, K. Gregory, A. Grübler, T. Y. Jung, T. Kram, E. L. La Rovere, L. Michaelis, S. Mori, T. Morita, W. Pepper, H. Pitcher, L. Price, K. Riahi, A. Roehrl, H.-H. Rogner, A. Sankovski, M. Schlesinger, P. Shukla, S. Smith, R. Swart, S. van Rooijen, N. Victor, Z. Dadi, Special report on emissions scenarios, A Special Report of Working Group III of the Intergovernmental Panel on Climate Change, Cambridge, UK (Jul. 2000).
- [13] J. Kniss, G. Kindlmann, C. Hansen, Multidimensional transfer functions for interactive volume rendering, *IEEE Transactions on Visualization and Computer Graphics* 8 (3) (2002) 270–285.
- [14] A. Inselberg, B. Dimsdale, Parallel coordinates: A tool for visualizing multi-dimensional geometry, in: *Proceedings of IEEE Visualization, 1990*, pp. 361–378.
- [15] E. Fanea, S. Carpendale, T. Isenberg, An interactive 3d integration of parallel coordinates and star glyphs, in: *Proceedings of IEEE Symposium on Information Visualization, IEEE Computer Society, Washington, DC, USA, 2005*, p. 20.
- [16] Y.-H. Fua, M. O. Ward, E. A. Rundensteiner, Hierarchical parallel coordinates for exploration of large datasets, in: *Proceedings of IEEE Visualization, IEEE Computer Society, Washington, DC, USA, 1999*.
- [17] C. W. Thornthwaite, An approach toward a rational classification of climate, *Geogr. Rev.* 38 (1) 55–94.
- [18] J. A. Hartigan, *Clustering Algorithms*, John Wiley & Sons, New York, 1975.
- [19] F. M. Hoffman, W. W. Hargrove, D. J. Erickson, R. J. Oglesby, Using clustered climate regimes to analyze and compare predictions from fully coupled general circulation models, *Earth Interact.* 9 (10) (2005) 1–27. doi:10.1175/EI110.1.
- [20] E. Saxon, B. Baker, W. Hargrove, F. Hoffman, C. Zganjar, Mapping environments at risk under different global climate change scenarios, *Ecol. Lett.* 8 (1) (2005) 53–60. doi:10.1111/j.1461-0248.2004.00694.x.
- [21] W. W. Hargrove, F. M. Hoffman, Potential of multivariate quantitative methods for delineation and visualization of ecoregions, *Environ. Manage.* 34 (Supplement 1) (2004) S39–S60. doi:10.1007/s00267-003-1084-0.
- [22] B. Baker, H. Diaz, W. Hargrove, F. Hoffman, Use of the Köppen-Trewartha climate classification to evaluate climatic refugia in statistically derived ecoregions for the People’s Republic of China, *Clim. Change* 98 (1) (2010) 113–131. doi:10.1007/s10584-009-9622-2.